INTERNATIONAL JOURNAL OF REFRIGERATION 60 (2015) 247–260

Available online at www.sciencedirect.com

ScienceDirect

journal homepage: www.elsevier.com/locate/ijrefrig

Dynamic model of a transcritical CO_2 ejector expansion refrigeration system

Lixing Zheng [a], *Jianqiang Deng* [a,*], *Yang He* [b], *Peixue Jiang* [c]

[a] *School of Chemical Engineering and Technology, Xi'an Jiaotong University, Xi'an 710049, China*

[b] *State Key Laboratory of Multiphase Flow in Power Engineering, Xi'an Jiaotong University, Xi'an 710049, China*

[c] *Key Laboratory for Thermal Science and Power Engineering, Department of Thermal Engineering, Tsinghua University, Beijing 100084, China*

ARTICLE INFO

Article history:
Received 4 November 2014
Received in revised form 22 July 2015
Accepted 25 August 2015
Available online 1 September 2015

Keywords:
Transcritical CO_2
Ejector expansion cycle
Dynamic modeling
Test validation

ABSTRACT

This paper presents a dynamic model of a transcritical CO_2 ejector expansion refrigeration cycle (EERC) which is a promising refrigeration system due to its environment-benign nature and low throttling loss. The mathematical models for gas cooler, evaporator and separator are formulated by using the mass and energy conservation equations. Based on the real properties of CO_2, the ejector model is developed and the variable ejector component efficiencies are taken into account because they vary with operation conditions. The compressor and expansive valve are modeled in a set of algebraic equations. The presented transient simulation results are in good agreement with the experimental data. The dynamic behaviors of the system undergoing the change of expansion valve opening and ejector area ratio are observed by the developed model, which helps to understand the characteristics of the EERC and guide the system control.

Modèle dynamique d'un système frigorifique à détente par éjecteur au CO2 transcritique

Mots clés : CO2 transcritique ; Cycle à détente par éjecteur ; Modélisation dynamique ; Validation de test

1. Introduction

Carbon dioxide is a promising refrigerant due to its environment-benign nature and extensive research efforts have been focused on the studies of transcritical CO_2 refrigeration system in recent years. A transcritical CO_2 ejector expansion refrigeration cycle (EERC) uses an ejector to replace expansion valve to recover throttling loss and increase cycle efficiency, making it attractive for the development of high-performance CO_2 refrigeration system. Many literatures performed thermodynamic analyses and steady state simulations with respect

* *Corresponding author.* School of Chemical Engineering and Technology, Xi'an Jiaotong University, Xi'an 710049, China. Tel.: +86 029 82663413; Fax: +86 029 82663413.
E-mail address: dengjq@mail.xjtu.edu.cn (J. Deng).

http://dx.doi.org/10.1016/j.ijrefrig.2015.08.019

Nomenclature

A	area [m^2]
COP	coefficient of performance
C_p	specific heat [J kg^{-1} K^{-1}]
D	diameter [m]
EERC	ejector expansion refrigeration cycle
h	specific enthalpy [J kg^{-1}]
EDL	equal-diameter length [mm]
L	length [m]
$\dot{m}$	mass flow rate [kg s^{-1}]
N	compressor rotational speed [r min^{-1}]
P	pressure [kPa]
s	specific entropy [J kg^{-1} K^{-1}]
T	temperature [°C]
u	internal energy [J kg^{-1}], velocity [m s^{-1}]
V	volume [m^3]
VCC	vapor compression cycle
v	velocity [m s^{-1}]
x	mass quality [–]
z	spatial variable along tube length [m]

Greek symbols

α	heat transfer coefficient [W m^{-2} K^{-1}]
γ	void fraction [–]
$\bar{\gamma}$	mean void fraction [–]
η	efficiency [–]
μ	entrainment ratio [–]
ρ	density [kg m^{-3}]

Subscripts

cal	calculation value
comp	compressor
cs	cross section
d	diffuser
e	evaporator
e1, e2	two-phase, superheated zone in evaporator
ej	ejector
ej0	initial state of ejector
f	saturated liquid
g	saturated vapor
gc	gas cooler
i	inner
in	inlet
int	interface of fluid region
is	isentropic
p	primary flow
mix	mixed flow
my	primary flow at the inlet of mixing section
n	nozzle
o	outer
ou	outlet
y	location where two streams start to mix
r	refrigerant
s	secondary flow
sw	shock wave
se	separator
sy	secondary flow at the inlet of mixing section
t	nozzle throat
total	total length of evaporator
v	expansion valve
v0	initial state of expansion valve
w	heat exchanger structure
wa	water

to the EERC (Deng et al., 2007; Li and Groll, 2005; Liu et al., 2012; Sarkar, 2008; Xu et al., 2012; Yari, 2009). However, the thermodynamic analysis cannot directly reflect the influence of structural parameters on the performance of the system. In addition, because the steady state simulations put particular emphasis on the static parameters such as COP and cooling capacity of system, they are not able to reveal how the parameters change over time. A dynamic simulation is an efficient approach to study the transient performances and optimize the structural parameters as well as operation conditions.

Generally, the transient models can be categorized into two classes: inductive and deductive models (Koury et al., 2013). The inductive models are based on a mathematical relation between the entry and exit variables of the system. The deductive models are based on the conservation equations of mass, momentum and energy and can be classified as global models and discretized models. In previous literatures the compressor is modeled by algebraic equations that are determined based on the inductive model and the same is true for expansion valves. For the heat exchanger model, Bendapudi and Braun (2002) pointed out that two different deductive modeling schemes were widely adopted: finite-volume distributed parameter and moving-boundary parameter. The moving-boundary approach divides the heat exchanger into different control zones corresponding to different heat transfer mechanisms, and the model parameters are obtained based on the laws of conservation. This approach is able to capture the dynamic characteristic of two-phase fluid and provide accurate transient predictions against experimental data, so it is widely adopted in transient simulation.

In the basis of the above methods, Rasmussen (2002) presented a model of a transcritical CO_2 vapor compression cycle (VCC). The system consisted of a gas cooler, an evaporator, an internal heat exchanger, an expansion valve, and a reciprocating compressor. The expansion valve and compressor were modeled with the algebraic relations, while the heat exchangers were developed with the moving-boundary parameter approach. And an experimental facility was set up to validate the dynamic model. The simulation results have a close agreement with the experimental data showing that the transient behavior could be accurately estimated by the proposed dynamic model. Pfafferott and Schmitz (2004) developed a Modelica library for CO_2-refrigeration system. The predicted pressure parameters showed a good agreement with the experiment while the mass flow rates differed considerably when the system was subjected to the disturbances of compressor speed step. Shi et al. (2010) developed a dynamic model of a transcritical CO_2 supermarket refrigeration system in Dymola

to investigate the system performance in the absence of physical prototypes.

Compared with the dynamic simulation of VCC, the EERC has an ejector resulting in the system coupling and solver to be more complex. In the EERC, the supercritical fluid from gas cooler flows into the primary nozzle of ejector and entrains the fluid from evaporator into the suction chamber. Then the two fluids mix and enter into the separator. The saturated vapor in separator is pumped into the compressor and the saturated liquid passes though the expansion valve into the evaporator. So the entire system is divided into two subcycles by the ejector and separator, and the input and output relationships among components become complicated. It is difficult to develop the model for each component, let alone an effective algorithm to integrate the models.

On the one hand, some complex thermodynamic phenomena existed in the ejector, such as the transonic flow, non-equilibrium phase change and two-phase flow shock wave. Several ejector mathematical models have already been presented based on 1D ideal gas dynamics theory and the principles of conservation of mass, momentum and energy (Chen et al., 2010, 2013; Eames et al., 1995; Huang et al., 1999). However, for a transcritical CO_2 ejector, if the gas dynamic theory is used and variable properties of CO_2 are also considered, it is easy to cause the calculation breakdown due to the property great change near by the critical point. More recent works have utilized CFD (Computational Fluid Dynamics) approach to study the ejector performance (Bartosiewicz et al., 2005; Chen et al., 2011; Little et al., 2012). Although the CFD method can accurately predict ejector performance, it is more complex and time consuming, requiring proper grid structuring and selection of a suitable turbulence model (Chen et al., 2013). However, a numerical model should balance the model complexity and the prediction accuracy.

Besides, the oscillatory motion of mixture–vapor transition point in evaporation process also needs to be paid close attention. Moreover, the robustness of ejector model depends on the succession of enthalpy and pressure of evaporator outlet. Especially, when the system is subjected to a large disturbance, the transition region of the two-phase flow in evaporator is easy to cross the enthalpy of the saturated vapor, which affects the downstream ejector. Zhang and Zhang (2006) introduced an evaporator model characterized by a time-dependent mean void fraction in the two-phase region showing an improved robustness and smoother state parameter curves during large transients.

On the other hand, the EERC includes a peculiar relation: the entrainment ratio μ and outlet mass quality x of ejector must satisfy the equilibrium as $(1+\mu)x=1$ under a steady condition (Cen et al., 2012; Deng et al., 2007; He et al., 2014; Li and Groll, 2005). If the equilibrium is not satisfied, the system will not operate steadily. When $(1+\mu)x>1$, the separator will accumulate excess steam resulting from the exorbitant of the outlet mass quality. When $(1+\mu)<1$, the outlet mass quality is lower and excessive liquid phase fluid flows into separator, which leads to the risk of compressor liquid strike.

This paper develops a numerical model to simulate the transient behavior of a transcritical CO_2 ejector expansion refrigeration cycle. A 1D transcritical CO_2 ejector model is developed based on the real properties. In addition, since ejector efficiencies vary with geometries and operation conditions, the variable ejector efficiencies are considered and embedded into the dynamic model. To avoid the effect of sudden change of evaporator parameters on the ejector, two evaporator models (one includes both two-phase region and superheated region while the other only includes the two-phase region) are developed respectively, and their smooth transition is dealt with employing the time-variant mean void fraction and weighted mean interface wall temperature of transition regions. Furthermore, a test rig is set up to obtain the experimental data and validate the model. The dynamic responses of the pressures of gas cooler, evaporator and separator, mass flow rates and entrainment ratio are simulated under the change of expansion valve opening and the ejector area ratio (the ratio of the area of mixing section to the area of primary nozzle throat).

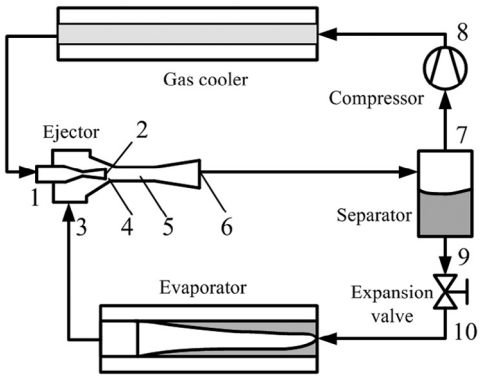

Fig. 1 – Schematic diagram of an EERC.

2. Mathematical model

A dynamic model of transcritical CO_2 EERC is constructed by a gas cooler, an ejector, an evaporator, an expansion valve, a separator and a compressor, as shown in Fig. 1. The corresponding cycle pressure–enthalpy diagram is shown in Fig. 2.

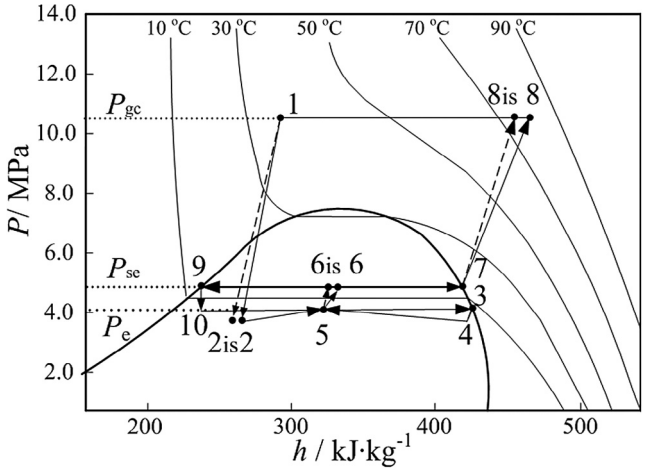

Fig. 2 – P–h diagram of an EERC.

The individual component models are firstly developed and then integrated them into the whole system dynamic model.

2.1. Compressor

A semi-hermetic reciprocating compressor is used in the system. The compression process is assumed as adiabatic and irreversible. Since the dynamical response of compressor evolves much smaller time scale than that of the heat exchanger, the operation is considered under steady state conditions. To calculate the refrigerant mass flow rate through the compressor $\dot{m}_{comp}$, the flowing equation is used (Sarkar et al., 2006):

$$\dot{m}_{comp} = \rho_{in}\eta_{vol}V\frac{N}{60} \quad (1)$$

where ρ_{in} is the refrigerant density at the compressor inlet, N, V and η_{vol} are the compressor rotational speed, the displacement volume and the volumetric efficiency, respectively. The η_{vol} is typically modeled using a semi-empirical relationship based on the pressure ratio and speed $\eta_{vol} = f(P_{ou}/P_{in}, N)$, where P_{in} and P_{ou} are the inlet and outlet pressures of compressor, respectively. The state of the fluid outlet is determined by assuming an isentropic efficiency η_{is}: $\eta_{is} = (h_{ou,is} - h_{in})/(h_{ou} - h_{in})$, where $h_{ou,is}$ is the outlet enthalpy of compressor assuming the isentropic process, h_{in} and h_{ou} are the actual inlet and outlet enthalpies of compressor, respectively.

2.2. Expansion valve

The expansion valve is assumed to be ideal throttling valves, and the expansion process is considered to be isenthalpic. For a fixed orifice expansion valves, the refrigerant flow rate is typically modeled using the correlation as Eq. 2 (Schurt et al., 2009).

$$\dot{m}_v = C_v A_{ev}\sqrt{2\rho_{in}(P_{in} - P_{ou})} \quad (2)$$

where C_v is the discharge coefficient determined empirically or from manufacturer information, A_{ev} is the effective passage flow area, $A_{ev} = A_0 A_v/100$, A_0 is the nominal orifice cross-sectional area, A_v is the valve opening (%), ρ_{in} is the refrigerant density at the valve inlet, P_{in} and P_{ou} are the inlet and outlet pressures of expansion valve.

2.3. Ejector

Fig. 3 shows a schematic of an ejector, which consists of a nozzle, a suction chamber, a mixing section and a diffuser. The high pressure primary flow expands and accelerates through the primary nozzle, and it flows out with supersonic speed resulting in a low pressure region at the nozzle exit (Cardemil and Colle, 2012; Chen et al., 2013). As a result of the differential pressure between the inlet of suction chamber and the exit of the primary nozzle, as well as the viscous entrainment effect, the secondary flow is entrained into the suction chamber. Then the two fluids mix and outflow the ejector through the diffuser. Since 1D model is computational cheap and easily integrated into system model (Chen et al., 2013), we develop a 1D two-phase ejector model. In the model, the flow is assumed

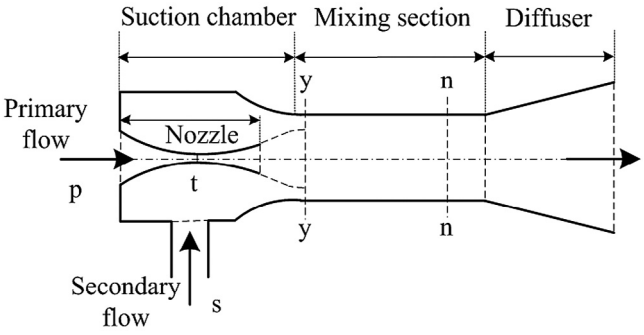

Fig. 3 – Schematic diagram of an ejector.

to be homogeneous equilibrium flow. The kinetic energies of the refrigerant at the ejector inlet and outlet are negligible. Under most working conditions, the fluid velocity can reach the speed of sound at the nozzle throat (White, 2009). Moreover, the operations of ejector are divided into three work modes, namely critical mode, sub-critical mode and back flow mode, respectively (Huang et al., 1999). Under the critical mode and sub-critical mode, the primary flows are all chocked, and at the back flow mode the secondary flow reverses, which is a meaningless working condition. Thus the primary flow is assumed to be chocked at nozzle throat. The critical flow does not occur for the secondary flow. The primary flow and the secondary flow achieve the same pressure at the inlet of constant-area mixing section and begin to mix with a uniform pressure (Cardemil and Colle, 2012). There is no mixing between the two fluids before reaching the inlet of the constant-area mixing section.

Fig. 4 displays the iterative flowchart of the two-phase CO_2 ejector calculation together with the governing equations based on the mass, momentum and energy conservation. The primary nozzle is divided into two sections, namely the converging section and the diverging section. The isentropic efficiency of converging section is defined as the primary nozzle efficiency η_n and another one of diverging section is assumed to be one (Cardemil and Colle, 2012). With an assumed value of the nozzle throat pressure P_t, using the primary nozzle inlet pressure P_p and enthalpy h_p as well as the isentropic efficiency η_n, the throat enthalpy h_t and velocity u_t are determined based on state equation and energy conservation equation. Because the primary flow is chocked, the velocity u_t must be equivalent to the speed of sound v_t. During the expansion of primary flow in the primary nozzle two-phase flow may develop, thus the calculation of two-phase sound speed should be employed. However, the evaluation of the two-phase sound speed is complex because the pressure and the temperature are not independent. In this study, the two-phase speed of sound is calculated referring to the literature by Cardemil and Colle (2012).

The velocity u_t is compared with sound speed v_t and the throat pressure P_t is updated until the two velocities are converged. After obtaining the throat velocity, the mass flow rate $\dot{m}_p$ through the primary nozzle throat can be obtained. To determine the inlet pressure of constant-area mixing section at

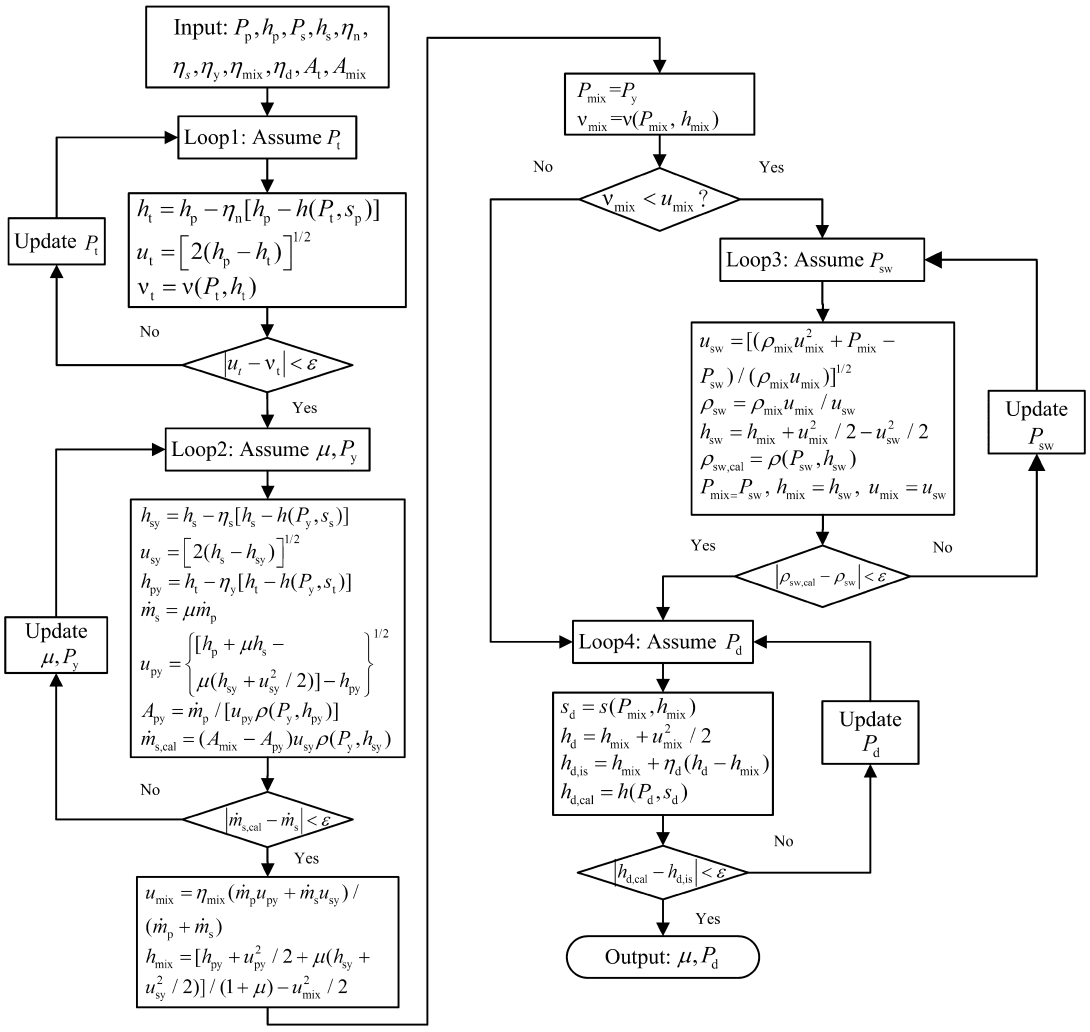

Fig. 4 – Flowchart for the simulation of two-phase ejector.

y–y cross section, the second iteration loop is applied. By initially assuming the inlet pressure P_y and entrainment ratio μ, using the suction nozzle inlet pressure P_s and enthalpy h_s as well as a suction nozzle efficiency η_s, the enthalpy h_{sy} and velocity u_{sy} of secondary flow at the inlet of constant-area mixing section are calculated based on the energy conservation equation and state equation. Similarly, the inlet enthalpy h_{py} and velocity u_{py} of primary flow at the same point are calculated. The primary flow expands in the suction chamber and the expansion process is considered using an isentropic efficiency η_y. The occupied area by the primary flow can be obtained and then the mass flow rate of secondary flow is calculated. The entrainment ratio μ and the inlet pressure P_y are obtained as mass conservation is satisfied. The pressure P_y is equal to the mixing pressure P_{mix}, and then the velocity u_{mix} and enthalpy h_{mix} of mixing flow are found by solving the conservation equations (mass and energy conservations) with the assumed mixing section efficiency η_{mix}. In order to check whether the flow in the two-phase mixing section occurred shock wave, the sound speed of two-phase mixing flow v_{mix} needs to be calculated. If the velocity u_{mix} is greater than v_{mix}, the shock wave happens assumed at n–n cross section and the state parameters after the wave can be calculated by virtue of mass, momentum and energy conservations. To determine the pressure of diffuser outlet P_d, the last iteration loop is applied. With the isentropic efficiency η_d, the entropy at the outlet of diffuser can be separately obtained based on the energy conservation equation and state equation. These two enthalpies are then compared and the diffuser outlet pressure P_d updates until the two enthalpies are converged.

Moreover, we need to know the efficiencies η_n, η_s, η_y, η_{mix} and η_d, which account for various losses in ejector. These efficiencies vary with ejector geometries and operation conditions, instead of the constant values. Liu and Groll (2013) combined experimental study with theoretical analysis to investigate the variable isentropic efficiencies of the primary nozzle, suction nozzle and the efficiency of mixing section. Their work challenged the traditional approach which assumed efficiency as a constant value. Since they have made such research, we did not need to spend much time and effort to do the similar work. However, because they did not directly supply the range of independent variables of the proposed correlations, it was easy

to exceed the reasonable range of efficiency 0–1.0 when they were directly applied. We dealt with these data to develop the correlations of isentropic efficiency on primary nozzle and suction chamber as follows:

$$\eta_n = 0.7797 + 0.5822\frac{D_t}{D_{mix}} - 0.1306\frac{p_p}{p_s} \tag{3}$$

$$\eta_s = -1.2075 - 0.1014\frac{D_t}{D_{mix}} + 0.9709\frac{p_p}{p_s} + 0.7318\left(\frac{D_t}{D_{mix}}\right)^2 - 0.1221\left(\frac{p_p}{p_s}\right)^2 \tag{4}$$

These correlations should be used within the following boundaries: $0.45 \le D_t/D_{mix} \le 0.675$, $2.0 \le P_p/P_s \le 4.5$.

2.4. Separator

The separator provides a storage volume, which is beneficial to ensure liquid into the expansion valve and vapor into the compressor. It is modeled as a simple control volume and the heat transfer is ignored between the wall and the surroundings. The separator pressure is assumed to be equal to the ejector outlet pressure. The conservation of mass and energy for the separator are written as Eqs. (5) and (6) (Eldredge et al., 2008).

$$\dot{m}_{se} = \dot{m}_{se,in} - (\dot{m}_{se,g} + \dot{m}_{se,f}) \tag{5}$$

$$\begin{aligned}&\left[\left(\frac{d\rho_{se,g}}{dP_{se}}V_{se,g}u_{se,g} + \frac{d\rho_{se,f}}{dP_{se}}V_{se,f}u_{se,f} + \frac{du_{se,g}}{dP_{se}}\rho_{se,g}V_{se,g} + \frac{du_f}{dP_{se}}\rho_{se,f}V_{se,f}\right)\right.\\ &\left.-\left(\frac{\rho_{se,g}u_{se,g} - \rho_{se,f}u_{se,f}}{\rho_{se,g} - \rho_{se,f}}\right)\left(\frac{d\rho_{se,g}}{dP_{se}}V_{se,g} + \frac{d\rho_{se,f}}{dP_{se}}V_{se,f}\right)\right]\\ &\frac{dP_{se}}{dt} + \left[\frac{\rho_{se,g}u_{se,g} - \rho_{se,f}u_{se,f}}{\rho_{se,g} - \rho_{se,f}}\right]\frac{dm_{se}}{dt}\\ &= \dot{m}_{se,in}h_{se,in} - \dot{m}_{se,g}h_{se,g} - \dot{m}_{se,f}h_{se,f}\end{aligned} \tag{6}$$

2.5. Heat exchanger

The evaporator and the gas cooler are the major components that most influence the transient performance of the system. Zhang and Zhang (2006) presented an evaporator model based on the moving-boundary method, and the model could predict the transient behaviors of evaporator under larger disturbances and kept the robustness whenever superheated region appeared or disappeared. Cecchinato and Mancini (2012) also developed an evaporator model which could switch between the two-zone (two-phase and superheat regions) and one zone (two-phase region). The switching algorithms adopted pseudo-state equations to track the inactive variables and ensure reasonable initial conditions. In addition, as discussed by Cecchinato and Mancini, the choice of the state variables was arbitrary but each solution lead to different consequences in the switching criteria and in the integrity conservation of the model. In this study, the evaporator model is developed according to the literature by Zhang and Zhang (2006). The first representation including two-phase and superheat regions is called TP-V model and the second one only with two-phase zone is TP model. Here for the TP-V model, the length of two-phase L_{e1}, pressure P_e, outlet enthalpy $h_{e,ou}$, two-phase wall temperature $T_{e1,w}$ and superheat zone wall temperature $T_{e2,w}$ are selected as variable. The pressure P_e, outlet enthalpy $h_{e,ou}$, and two-phase wall temperature $T_{e1,w}$ are chosen for the TP model.

A number of assumptions must be made to reduce the complexity of the conservation equations (Rasmussen, 2002; Zhang and Zhang, 2006): (1) The fluid flow is one-dimensional. (2) Pressure drop of the fluid flow is negligible. (3) There is no axis thermal heat conduction in the fluid flow and in the tube wall. The PDEs (Partial Differential Equations) for conservation of refrigerant mass and energy are represented in Eqs. (7) and (8). The z-coordinate specifies a location along the length of the heat exchanger.

$$\frac{\partial(\rho A_{cs})}{\partial t} + \frac{\partial \dot{m}}{\partial z} = 0 \tag{7}$$

$$\frac{\partial(\rho A_{cs}h - A_{cs}p)}{\partial t} + \frac{\partial(\dot{m}h)}{\partial z} = \alpha_i \pi D_i (T_w - T_r) \tag{8}$$

Eq. (7) is the differential continuity equation for unidirectional flow in the z direction. Eq. (8) presents the differential conservation of energy, which states that the rate of energy variation in the refrigerant is due to changes in enthalpy, pressure and position (Eldredge et al., 2008).

2.5.1. TP-V model

In this case, both the two-phase and superheated regions exist in the evaporator. Because the moving-boundary derivation requires the integration of the PDEs, the conservation equations of refrigerant mass and energy presented by Eqs. (7) and (8) are integrated in the two-phase region and superheated region, respectively, to obtain four corresponding DAEs (Differential Algebraic Equations) using the Leibniz integration rule. Since the outlet of two-phase region is the inlet of superheated region, combining the two equations of mass conservation for the two-phase region and superheated region can eliminate the interface mass flow rate $\dot{m}_{int}$ and the result is showed in Eq. (9). For the two-phase region, substituting the interface mass flow rate from mass conservation equation into the energy conservation equation yields Eq. (10). Similarly, substituting the interface mass flow rate from mass conservation equation into the energy conservation for the superheated region yields Eq. (11). Here DAEs for the refrigerant in the TP-V model are represented in their final form, and the details about the derivation process can be found in the literature by Zhang and Zhang (2006).

$$\begin{aligned}&\left\{\left[\frac{d\rho_{e,f}}{dP_e}(1-\bar{\gamma}) + \frac{d\rho_{e,g}}{dP_e}\bar{\gamma} + (\rho_{e,g} - \rho_{e,f})\frac{\partial\bar{\gamma}}{\partial P_e}\right]L_{e1} + \frac{\partial\rho_{e2}}{\partial p_e}L_{e2}\right\}A_{e,cs}\frac{dP_e}{dt}\\ &+ [(\rho_{e,g} - \rho_{e,f})(\bar{\gamma} - 1) + (\rho_{e,g} - \rho_{e2})]A_{e,cs}\frac{dL_{e1}}{dt}\\ &+ \frac{\partial\rho_{e2}}{\partial h_{e,ou}}A_{e,cs}L_{e2}\frac{dh_{e,ou}}{dt} = \dot{m}_{e,in} - \dot{m}_{e,ou}\end{aligned} \tag{9}$$

$$\begin{aligned}&\left[\left(\frac{d(\rho_{e,f}h_{e,f})}{dP_e}-\frac{d\rho_{e,f}}{dP_e}h_{e,g}\right)(1-\bar{\gamma})+\left(\frac{dh_{e,g}}{dP_e}\rho_{e,g}\right)\bar{\gamma}\right.\\&\left.+\rho_{e,f}(h_{e,g}-h_{e,f})\frac{\partial\bar{\gamma}}{\partial P_e}-1\right]A_{e,cs}L_{e1}\frac{dP_e}{dt}\\&+[(\rho_{e,f}(h_{e,f}-h_{e,g})(1-\bar{\gamma})]A_{e,cs}\frac{dL_{e1}}{dt}\\&=\dot{m}_{e,in}(h_{e,in}-h_{e,g})+\alpha_{e1,i}A_{e,i}\left(\frac{L_{e1}}{L_{total}}\right)(T_{e1,w}-T_{e1,r})\end{aligned}\tag{10}$$

$$\begin{aligned}&\left(\frac{\partial(\rho_{e2}h_{e2})}{\partial P_e}-\frac{\partial\rho_{e2}}{\partial P_e}h_{e,g}-1\right)A_{e,cs}L_{e2}\frac{dP_e}{dt}+\rho_{e2}(h_{e,g}-h_{e2})A_{e,cs}\frac{dL_{e1}}{dt}\\&+\left(\frac{\partial(\rho_{e2}h_{e2})}{\partial h_{e,ou}}-\frac{\partial\rho_{e2}}{\partial h_{e,ou}}h_{e,g}\right)A_{e,cs}L_{e2}\frac{dh_{e,ou}}{dt}=\dot{m}_{e,ou}(h_{e,g}-h_{e,ou})\\&+\alpha_{e2,i}A_{e,i}\left(\frac{L_{e2}}{L_{total}}\right)(T_{e2,w}-T_{e2,r})\end{aligned}\tag{11}$$

2.5.2. TP model

Since in this case the two-phase region occupies the whole evaporator and the outlet state of refrigerant flow is two-phase, the equations of refrigerant mass and energy are integrated and the results are shown as follows:

$$\begin{aligned}&\left[\frac{d\rho_{e,f}}{dP_e}(1-\bar{\gamma})+\frac{d\rho_{e,g}}{dP_e}\bar{\gamma}+(\rho_{e,g}-\rho_{e,f})\frac{\partial\bar{\gamma}}{\partial P_e}\right]A_{e,cs}L_{total}\frac{dP_e}{dt}\\&+\frac{\rho_{e,g}-\rho_{e,f}}{h_{e,g}-h_{e,f}}\frac{\partial\bar{\gamma}}{\partial x_{int}}A_{e,cs}L_{total}\frac{dh_{e,ou}}{dt}=\dot{m}_{e,in}-\dot{m}_{e,ou}\end{aligned}\tag{12}$$

$$\begin{aligned}&\left\{\frac{d(\rho_{e,f}h_{e,f})}{dP_e}(1-\bar{\gamma})+\left(\frac{d(\rho_{e,g}h_{e,g})}{dP_e}\right)\bar{\gamma}+(\rho_{e,g}h_{e,g}-\rho_{e,f}h_{e,f})\frac{\partial\bar{\gamma}}{\partial P_e}-1\right\}\\&A_{e,cs}L_{total}\frac{dP_e}{dt}+\left[\left(\frac{\rho_{e,g}h_{e,g}-\rho_{e,f}h_{e,f}}{h_{e,g}-h_{e,f}}\right)\frac{\partial\bar{\gamma}}{\partial x_{int}}\right]A_{e,cs}L_{total}\frac{dh_{e,ou}}{dt}\\&=\dot{m}_{e,in}h_{e,in}-\dot{m}_{e,ou}h_{e,ou}+\alpha_{e1,i}A_{e,i}(T_{e1,w}-T_{e1,r})\end{aligned}\tag{13}$$

2.5.3. Tube wall model

According to previous assumptions, the governing equation of the tube wall is the energy equation. The PDE for conservation of tube wall energy is given in Eq. (14). This equation shows the rate of energy change in the wall, because temperature variations must equal to the rate of heat transfer between the wall and the refrigerant as well as the surrounding water (Eldredge et al., 2008). Integrating Eq. (14) over the two-phase and superheated regions, we have Eqs. (15) and (16):

$$(C_p\rho A)_w\frac{\partial T_w}{\partial t}=\alpha_i\pi D_i(T_r-T_w)+\alpha_o\pi D_o(T_{wa}-T_w)\tag{14}$$

$$\begin{aligned}\rho_{e,w}A_{e,w}C_{p,w}\int_0^{L_{e1}}\frac{\partial T_{e1,w}}{\partial t}dz=&(-\alpha_{e1,i}A_{e,i}(T_{e1,w}-T_{e1,r})\\&-\alpha_{e,o}A_{e,o}(T_{e1,w}-T_{e1,wa}))L_{e1}\end{aligned}\tag{15}$$

$$\begin{aligned}\rho_{e,w}A_{e,w}C_{p,w}\int_{L_{e1}}^{L_{e2}}\frac{\partial T_{e2,w}}{\partial t}dz=&(-\alpha_{e2,i}A_{e,i}(T_{e2,w}-T_{e2,r})\\&-\alpha_{e,o}A_{e,o}(T_{e2,w}-T_{e2,wa}))L_{e2}\end{aligned}\tag{16}$$

2.5.4. Transition between TP-V and TP models

The mean property of refrigerant plays a key role to make the simulation result continuous and smooth. In the studies of Rasmussen (2002) and Rasmussen et al. (2005), the void fraction is used to constant and the integration $\int_0^{L_{e1}}(\partial\gamma/\partial t)dz$ is written as Eq. (17). However, it shows that the value of the integration is discontinuous when L_{e2} approaches zero, which leads to the sudden change in outlet enthalpy and its derivatives.

$$\int_0^{L_{e1}}\left(\frac{\partial\gamma}{\partial t}\right)dz=\begin{cases}(\bar{\gamma}-1)\dfrac{dL_{e1}}{dt} & L_{e2}>0\\ 0 & L_{e2}=0\end{cases}\tag{17}$$

Thus herein the integration $\int_0^{L_{e1}}(\partial\gamma/\partial t)dz$ is derived as Eq. (18), which is continuous when L_{e2} approaches zero because it is based on the integration method without omitting any items (Zhang and Zhang, 2006).

$$\int_0^{L_{e1}}\left(\frac{\partial\gamma}{\partial t}\right)dz=\begin{cases}L_{e1}\dfrac{\partial\bar{\gamma}}{\partial p_e}\dfrac{dp_e}{dt}+(\bar{\gamma}-1)\dfrac{dL_{e1}}{dt} & L_{e2}>0\\ L_{e1}\left(\dfrac{\partial\bar{\gamma}}{\partial p_e}\dfrac{dp_e}{dt}+\dfrac{1}{h_{e,g}-h_{e,f}}\dfrac{\partial\bar{\gamma}}{\partial x_{int}}\dfrac{dh_{e,ou}}{dt}\right) & L_{e2}=0\end{cases}\tag{18}$$

In above equations, the mean void fraction captures the relationship between vapor mass and liquid mass in the two-phase region, and it determines the outlet enthalpy and fluid properties. Many void fraction models have been developed under different experimental setup and conditions (Rice, 1987). Rasmussen (2002) developed a dynamic model on the transcritical CO_2 vapor compression system, and the mean void fraction was estimated by the following equation:

$$\bar{\gamma}=\frac{1}{\beta}+\frac{1}{x_{out}-x_{in}}\left[\frac{\alpha}{\beta^2}\ln\left(\frac{\beta x_{in}+\alpha}{\beta x_{out}+\alpha}\right)\right]\tag{19}$$

Where $\alpha=\left(\frac{\rho_g}{\rho_f}\right)S$, $\beta=1-\alpha$, S is slip ratio. Moreover, the model effectiveness was validated by the experimental data and the results show that the predictions were agreed well with the experimental data. Here the mean void fraction is calculated referring to the literature by Rasmussen (2002).

In addition, the wall temperature at the interface of two regions is another important factor for robust continuity. Some investigators (Pettit et al., 1998; Rasmussen, 2002) regarded the interface as part of the two-phase region, namely $T_{w,int}=T_{e1,w}$. However, when the superheated region disappears, L_{e2} will approach zero ahead of dL_{e2}/dt and leads to failing to get the true values of dL_{e2}/dt and $T_{e2,w}$ (Zhang and Zhang, 2006). Jesen and Tummescheit (2002) adopted another modified form to get more reasonable results.

$$T_{w,int}=\begin{cases}T_{e2,w} & \dfrac{dL_{e1}}{dt}>0\\ T_{e1,w} & \dfrac{dL_{e1}}{dt}\le 0\end{cases}\tag{20}$$

Although this can avoid the unreasonable trends of $T_{e2,w}$ when L_{e2} approach zero, they cannot keep the smooth transition, especially the transition between the TP-V model and the TP model. So the interface wall temperature is assumed as a weighted mean of $T_{e1,w}$ and $T_{e2,w}$, as follows (Zhang and Zhang, 2006):

$$T_{w,int} = \frac{L_{e2}}{L_{total}} T_{e1,w} + \frac{L_{e1}}{L_{total}} T_{e2,w} \tag{21}$$

This representation is closer to the practical situation. It implies that if L_{e1} increases, the interface temperature is close to $T_{e2,w}$ because of the superheated region over there, and vice versa. Moreover, Eq. (21) has the same advantage of Eq. (20) and can guarantee the robust transition between the TP-V model and TP model. Substituting Eq. (21) into Eqs. (15) and (16), the symmetric and robust expression of wall temperatures can be obtained:

$$\rho_{e,w}A_{e,w}C_{p,w}\left(\frac{dT_{e1,w}}{dt} + \frac{T_{e1,w}-T_{e2,w}}{L_{total}}\frac{dL_{e1}}{dt}\right) = -\alpha_{e1,i}A_{e,i}(T_{e1,w}-T_{e1,r}) - \alpha_{e,o}A_{e,o}(T_{e1,w}-T_{e1,wa}) \tag{22}$$

$$\rho_{e,w}A_{e,w}C_{p,w}\left(\frac{dT_{e2,w}}{dt} + \frac{T_{e1,w}-T_{e2,w}}{L_{total}}\frac{dL_{e1}}{dt}\right) = -\alpha_{e2,i}A_{e,i}(T_{e2,w}-T_{e2,r}) - \alpha_{e,o}A_{e,o}(T_{e2,w}-T_{e2,wa}) \tag{23}$$

The calculation of gas cooler is simpler than the case of the evaporator because there is only supercritical phase. For the gas cooler, the pressure P_{gc}, the mean enthalpy h_{gc} and the tube wall temperature $T_{gc,w}$ are chosen as variables. The PDEs for conservation of refrigerant mass and energy shown in Eqs. (7) and (8) are integrated along the length of gas cooler and the results are written as:

$$A_{gc,cs}L_{gc}\left(\frac{\partial\rho_{gc}}{\partial P_{gc}}\right)\frac{dP_{gc}}{dt} + A_{gc,cs}L_{gc}\left(\frac{\partial\rho_{gc}}{\partial h_{gc}}\right)\frac{dh_{gc}}{dt} = \dot{m}_{gc,in} - \dot{m}_{gc,ou} \tag{24}$$

$$\left[\left(\frac{\partial\rho_{gc}}{\partial P_{gc}}\right)h_{gc}+1\right]A_{gc,cs}L_{gc}\frac{dP_{gc}}{dt} + \left[\left(\frac{\partial\rho_{gc}}{\partial h_{gc}}\right)h_{gc}+\rho_{gc}\right]A_{gc,cs}L_{gc}\frac{dh_{gc}}{dt} = \dot{m}_{gc,in}h_{gc,in} - \dot{m}_{gc,ou}h_{gc,ou} + \alpha_{gc,i}D_{gc,i}L_{gc}(T_{gc,w}-T_{gc,r}) \tag{25}$$

Integrating Eq. (14) for energy conservation of tube wall results in:

$$\rho_{gc,w}A_{gc,w}C_{p,w}\frac{d(T_{gc,w})}{dt} = \alpha_{gc,i}A_{gc,i}(T_{gc,r}-T_{gc,w}) - \alpha_{gc,o}A_{gc,o}(T_{gc,w}-T_{gc,wa}) \tag{26}$$

2.6. *Solution algorithm*

The overall system simulation relies on the above component models. The entire EERC is divided into two sub-cycles by the ejector and gas–liquid separator, and the coupling among physical parameters is intricate and complex shown in Fig. 5. To simplify the analysis, the following assumptions are considered in the simulation: (1) Heat transfer with the ambient is negligible. (2) The pressure drop in connecting pipes is neglected. (3) The working fluid flow is one-dimensional and homogeneous equilibrium flow. To solve the closed cycle, it is necessary to know the calculation starting. In the six components, the state parameters of compressor, expansion valve and ejector do not vary at each calculation step while gas cooler, evaporator and separator adopt time-variable dynamic model and their parameters change at each calculation step. Furthermore, according to the character of the moving-boundary

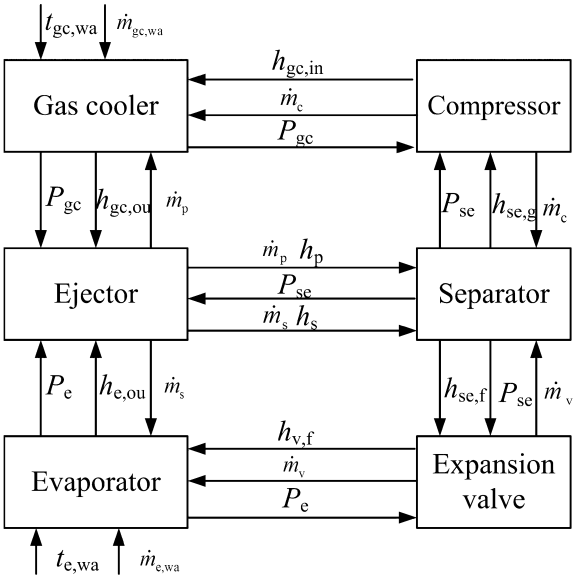

Fig. 5 – Physical parameters coupling of EERC.

method, the state parameters are obtained based on the inlet and outlet mass flow rates, so the models of compressor, expansion valve and ejector are firstly calculated and then the results are as the input of the models of gas cooler, evaporator and separator at each calculation step. It is worth noting that during the evaporator calculations, the computed value of the outlet enthalpy must be compared with the saturated vapor enthalpy value to determine whether the transition from single to two-phase flow occurs or not. The flowchart of system dynamic simulation is shown in Fig. 6. The numerical integrations of the differential equations are carried out through the fourth order Runge–Kutta method. The thermodynamic properties are obtained from REFPROP 7.0 (McLinden et al., 2002).

3. Model validation

3.1. *Experimental setup*

A schematic of the experimental setup is given in Fig. 7. The compressor was a prototype semi-hermetic reciprocating type compressor and was manufactured by Dorin. An inverter was used to change the compressor frequency. The gas cooler and evaporator were counter-flow type heat exchanger with concentric dual tubes, which were made of copper and were wound into spiral coils. In the heat exchanger, the refrigerant flowed through the inner tubes and the water flowed through the annulus counter-currently to the refrigerant. The detail structure parameters are displayed in Table 1.

The experimental ejector was adjustable and some structure parameters could be regulated such as primary nozzle throat area, the distance between the outlet of primary nozzle and the inlet of mixing section and the diameter of mixing section. It needed to be pointed out that the ejector nozzle was not the convergence–divergence but the convergence and with an equal-diameter section. The equal-diameter length (EDL) section could also be made into different dimensions. The

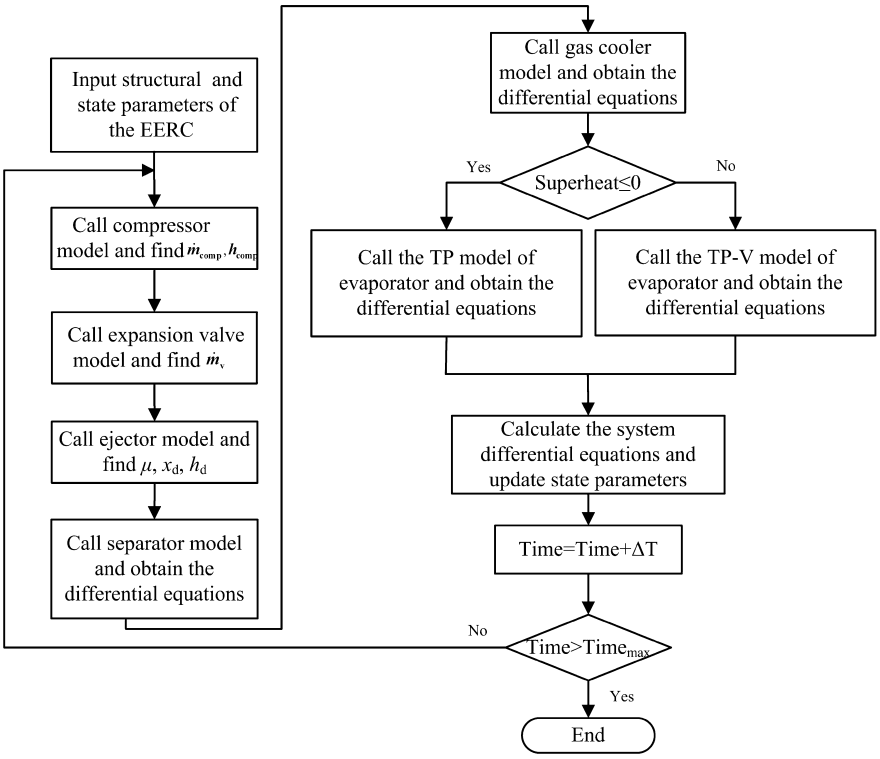

Fig. 6 – Flowchart of the dynamic simulation of EERC.

separator was installed after the ejector to serve as a buffer of refrigerant, and to improve the system performance as well as avoid damage to the compressor. The expansion valve was a metering valve whose maximum working pressure was 20.6 MPa at 37 °C and was manufactured by Swagelok. In the validation, some parameters and geometric data of the experimental components are presented in Table 1.

The uncertainties of the experimental data were mainly from the measurement error and the data acquisition error. The temperature and pressure in the setup were measured using thermocouples, resistance temperature detectors (RTDs) and pressure transducers. The accuracy of the thermocouples and RTDs was ±0.5 °C and ±0.15 °C, respectively, while the accuracy of the pressure transducer was ±0.075% of the full scale, and the absolute accuracy for the pressure of gas cooler, separator and evaporator was 11.25 kPa, 4.5 kPa and 4.5 kPa, respectively. Mass flow meters based on Coriolis effect were used to measure the refrigerant mass flow rate of primary flow and secondary flow, whose accuracy was ±0.1% of the full scale, and the absolute accuracy for the primary flow and suction flow was 0.097 g s^{-1} and 0.069 g s^{-1}, respectively. Because the ratio of primary mass flow rate to the secondary mass flow rate was defined as the entrainment ratio, its uncertainty was obtained indirectly based on that of mass flow rate of primary flow and secondary flow. The data acquisition error is very smaller than the measurement error and can be ignored. Thus,

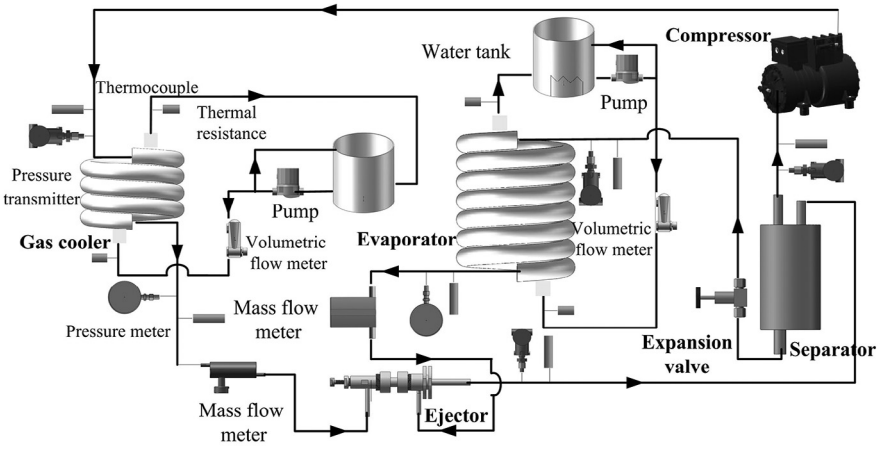

Fig. 7 – Schematic diagram of experimental apparatus.

Table 1 – Some parameters and geometric data of the experimental components.

Parameters	Value	Parameters	Value
Gas cooler		EDL	0.006 m
Length	3.5 m	Separator	
Internal/external diameter of inner tube	0.006 m/0.01 m	Diameter	0.164 m
Internal/external diameter of outer tube	0.013 m/0.016 m	Height	0.35 m
Evaporator		Expansion valve	
Length	5.0 m	Opening	25%
Internal/external diameter of inner tube	0.007 m/0.01 m	Compressor	
Internal/external diameter of outer tube	0.016 m/0.018 m	Displacement	1.46 m^3h^{-1}
Ejector		Nominal rotation	1450 r min^{-1}
Area ratio	3.63		

the uncertainty of the experimental data is summarized in Table 2.

Before the comparison between the experimental results and numerical simulation, some component models should be amended according to the experimental data, such as the volume efficiency and isentropic efficiency of compressor, the flow coefficient of expansion valve, and the heat transfer coefficients of refrigerant and water. Eqs. (27) and (28) show the fitting correlations of volume efficiency and isentropic efficiency of compressor. According to the two equations, the values of volumetric and isentropic efficiencies are smaller under the experimental conditions. This could be explained that the working conditions in the experiment deviate from efficient working conditions of the compressor. And the wear of components may lead to the efficiencies of compressor decrease.

$$\eta_{vol} = 0.7711 - 0.1043\frac{P_{gc}}{P_{se}} \quad (27)$$

$$\eta_{is} = 0.21 + 0.1556\frac{P_{gc}}{P_{se}} \quad (28)$$

The water-to-structure heat transfer coefficient was calculated by the correlations proposed by Gnielinski (1976). The two-phase refrigerant heat transfer correlation developed by Hwang (1997) was chosen and the correlation presented by Dang and Hihara (2004) was applied for the calculation of single phase refrigerant heat transfer. The heat transfer coefficients were updated with the experimental operating conditions. More precisely, the refrigerant and water side heat transfer coefficient of the gas cooler were reduced by 20% and the two-phase region heat transfer coefficient including the refrigerant and water sides were enlarged by 20%. For the expansion valve, the flow coefficient was 0.37 according to the manufacturer. The efficiencies of primary nozzle and suction chamber were estimated by the correlations Eqs. (3) and (4). Observing the experimental data listed in literature by Liu and Groll, 75% of mixing efficiency was in the scope of 0.9–1.0, so the mean value of 0.95 was used as the mixing efficiency. The efficiency indicating the expansion process of primary flow in suction chamber was assumed as 0.95 (Cardemil and Colle, 2012). And the diffuser efficiency was assumed as 0.85. However, it needs to be pointed out that the diffuser efficiency may not be required for the dynamic simulation of EERC because the back pressure of ejector is calculated by the model of separator.

3.2. *Validation results*

The compressor speed N was chosen as the disturbance to validate the simulation results. The initial operation conditions were shown in Table 3. Figs. 8 and 9 show the contrastive results between the experimental data and simulation predictions. In Figs. 8 and 9, when the compressor speed was changed from 1500 r min^{-1} to 1200 r min^{-1}, the displacement of compressor rapidly reduced and the mass flow rate into the gas cooler decreased, resulting in the decrease in pressure of gas cooler. Due to the decrease of the suction flow rate of compressor, the storage of separator increased and its pressure increased. As the inlet pressure of primary nozzle (i.e. gas cooler pressure) decreased, the primary flow rate was decreased and lead to the secondary flow rate decrease as well as the evaporator pressure increase. Although both the primary flow rate and secondary flow rate decreased, the variation of secondary flow rate was smaller than that of primary flow rate and lead to the

Table 2 – Measurement uncertainties of experimental data.

Parameters	Uncertainty	Description
Temperature (refrigerant)	±0.29 °C	Inlet and outlet of heat exchangers
Pressure (refrigerant)	$\pm 2.60 \times 10^{-3}$ MPa	Evaporator and separator pressure
	$\pm 6.50 \times 10^{-3}$ MPa	Gas cooler pressure
Mass flow meter (refrigerant)	$\pm 5.61 \times 10^{-6}$ kg s^{-1}	Primary flow
	$\pm 4.0 \times 10^{-6}$ kg s^{-1}	Secondary flow
Entrainment ratio	$\pm 3.90 \times 10^{-4}$	
Temperature (water)	±0.087 °C	Inlet and outlet of heat exchangers
Volume flow rate (water)	±0.023 L min^{-1}	Chilled water
	±0.023 L min^{-1}	Cooling water
Diameter	±0.012 mm	Diameter of needle at the inlet of nozzle

Table 3 – Model validation operating conditions.

Parameters	Unit	Value	Parameters	Unit	Value
Gas cooler			Inlet enthalpy	kJ kg^{-1}	198.02
Pressure	MPa	8.596	Outlet enthalpy	kJ kg^{-1}	458.24
Inlet enthalpy	kJ kg^{-1}	492.5	Mass flow rate	g s^{-1}	10.1
Outlet enthalpy	kJ kg^{-1}	297.3	Water inlet temperature	°C	19.54
Mass flow rate	g s^{-1}	19.58	Water mass flow rate	kg s^{-1}	0.097
Water inlet temperature	°C	19.57	Ejector		
Water mass flow rate	kg s^{-1}	0.042	Outlet pressure	MPa	3.408
Evaporator			Outlet enthalpy	kJ kg^{-1}	462.2
Pressure	MPa	3.21	Entrainment ratio		0.516

increase of entrainment ratio. Then, with the rise of separator pressure and evaporator pressure, the differential pressure between the separator and gas cooler decreased, which lead to the increase in mass flow rate of compressor. Similarly, the differential pressure between the separator and evaporator declined resulting in the decrease in mass flow rate of expansion valve. The system gradually restores stability through its autoregulation. For the increase of compressor speed, the parameters of system showed a reverse trend to that of the compressor speed decrease.

In Fig. 8, although the predicted pressure changed rapidly than that of the experiment, the predictions had the similar tendencies with the experimental results and when the system restored to steady state the relative error for gas cooler pressure, evaporator pressure and separator pressure was 1.8%, 4.2% and 6.7%, respectively. In Fig. 9, the curves of entrainment ratio corresponding to prediction and experiment were of fair agreement. By contrast, the comparison of primary flow rate presented larger difference. Some factors which contribute to the prediction deviation may be:

(1) the pressure loss in the heat exchangers and connection pipes was omitted leading to the higher steady state pressure with respect to the model simulation;
(2) in the experimental components there was some lubricating oil circulating together with the refrigerant, and the adopted correlations did not represent adequately the experimental situation, resulting in the distinction of heat transfer coefficient;
(3) the compressor, the expansion valve and the ejector model were developed based on the 1D method, especially the compressor and expansion valve using algebraic equations instead of physical models. Moreover, the uncertainty of component-specific parameters such as compressor efficiencies, sound speed of two-phase fluid and the ejector efficiencies affected the simulation precision as well as the time response.

4. Simulation and results

In the following, results of the transient simulation of the above mentioned EERC are presented. The expansion valve opening and the area ratio of ejector (the mixing section area to the primary nozzle throat area) are set as the boundary conditions. The expansion valve opening and the area ratio of ejector relative to the initial state, namely A_v/A_{v0} and A_{ej}/A_{ej0}, are changed as shown in Fig. 10. In Fig. 10, the A_v/A_{v0} rising from 1.0 to 1.4 means that the expansion valve opening increases by one circle in the real experimental apparatus, namely the expansion valve opening change from 25% to 35%. When the A_{ej}/A_{ej0} changes from 1.0 to 1.24, it means that the ejector area ratio increases from the initial valve of 3.63 to 4.5. The reason we chose the ejector area ratio value of 4.5 is that the ejector shows the optimal performance under the conditions.

The pressure of gas cooler, separator and evaporator varying with time are shown in Fig. 11. It can be found that when the opening of expansion valve increases, the gas cooler pressure reduces while the pressures of separator and evaporator rise. For the area ratio of ejector, when it increases, the gas cooler pressure rises while the pressures of separator and evaporator decrease. Thus, the increase or decrease of valve opening has the similar trends with the decrease or increase of ejector area ratio for the pressure parameter response. The

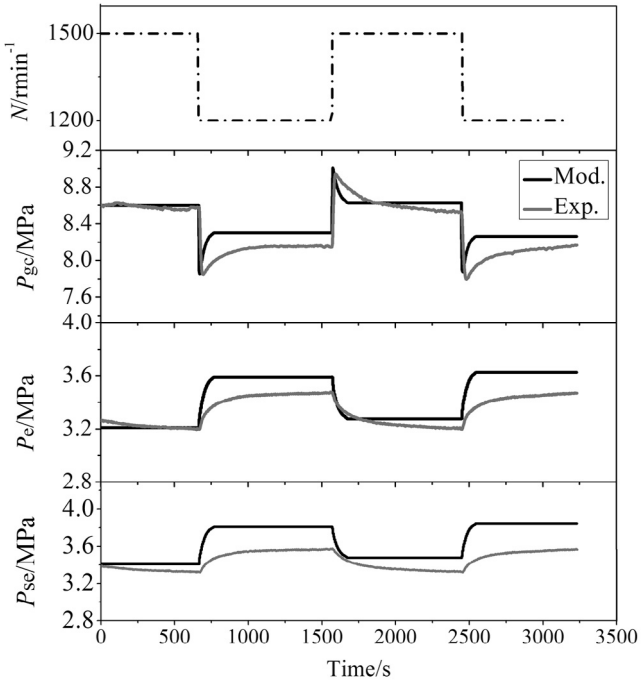

Fig. 8 – Model validation: the pressure of gas cooler, evaporator and separator for step change in compressor speed.

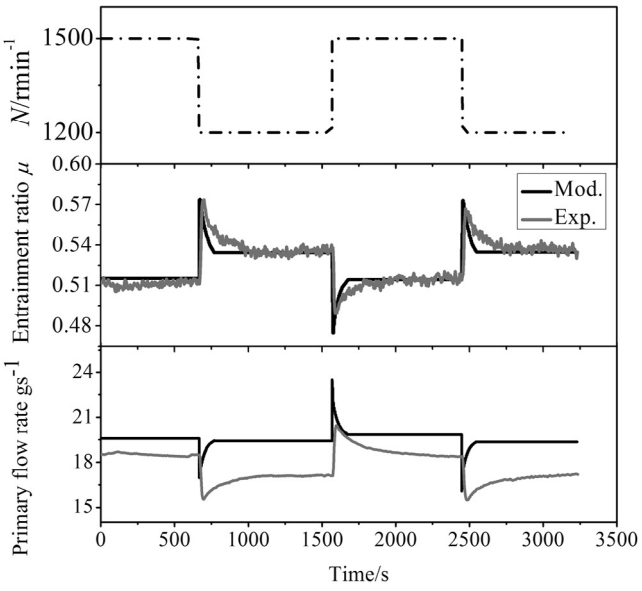

Fig. 9 – Model validation: entrainment ratio and primary flow rate for step change in compressor speed.

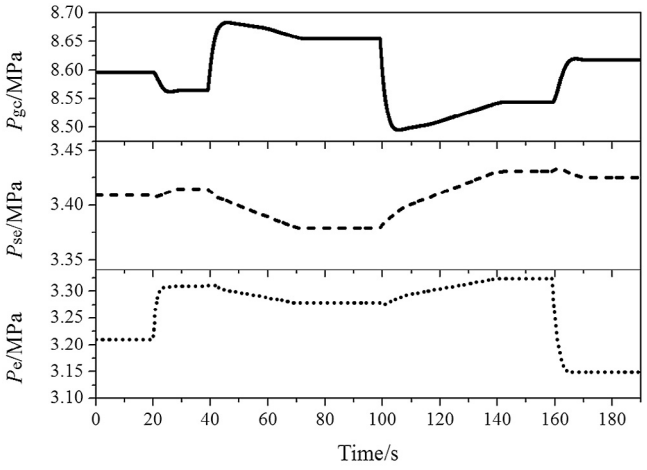

Fig. 11 – Pressure of gas cooler, separator and evaporator vs. time.

gas cooler pressure appears overshoot under the changes of expansion valve opening and area ratio of ejector. In addition, the area ratio of ejector has greater effect on gas cooler pressure while the expansion valve opening influences the evaporator pressure more greatly. This phenomenon is attributed to the separating effect of the ejector as mentioned above. Thus a control strategy is proposed: to obtain a fixed gas cooler pressure, the area ratio of the ejector is suggested to be controlled; for the evaporator pressure, the valve opening is recommended.

Fig. 12 shows the variation of mass flow rates in expansion valve and ejector secondary flow. From Fig. 12, the mass flow rate of expansion valve increases significantly after the expansion valve opening increase. However, when the system reaches the steady state, the change of mass flow rates is small. For the increase of area ratio of the ejector, the mass flow rate of expansion valve decreases. Thus, the mass flow rate of secondary flow has the similar varying tendency with the expansion valve flow rate when the expansion valve opening changes or the area ratio of the ejector does, but the variations after stability are minor. Fig. 13 displays the change of mass flow rates in compressor and ejector primary flows. The primary flow rate appears overshoot under the change of expansion valve opening and area ratio of the ejector, and it increases with the increase of expansion valve opening or the decrease of ejector area ratio. The compressor flow rate has the similar trends with the primary flow rate. Combining Figs. 12 and 13, when the area ratio of ejector increases, although both the primary flow and secondary flow decrease, the variation of secondary flow is smaller than that of primary flow and leads to the increase of entrainment ratio as shown in Fig. 14. Moreover, the change of entrainment ratio follows similar trends with the variation of expansion valve opening and area ratio of the ejector. Another major performance parameter of ejector, pressure lift ratio, which is the ratio of separator pressure to evaporator pressure, is also shown in Fig. 14. It can be found

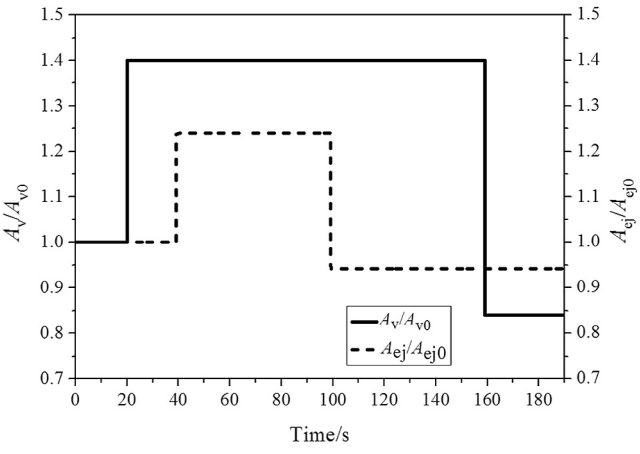

Fig. 10 – Change of valve opening and area ratio in ejector as the boundary conditions of simulation.

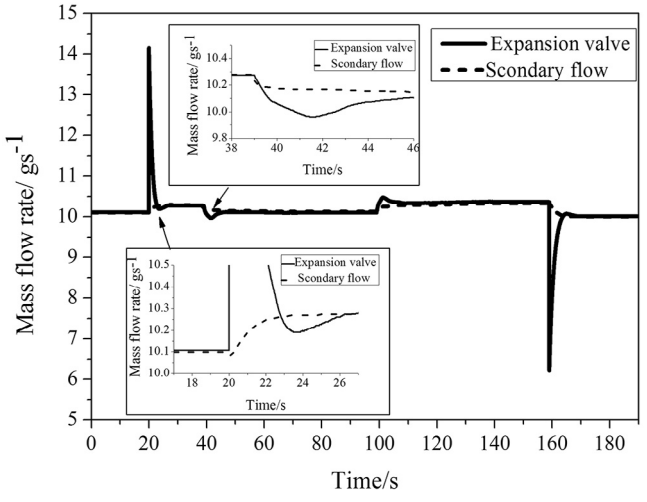

Fig. 12 – Mass flow rates of expansion valve and secondary flow of ejector vs. time.

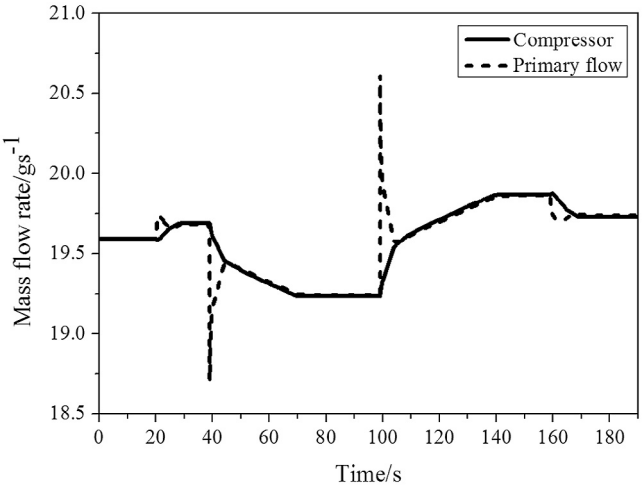

Fig. 13 – Mass flow rates of compressor and primary flow of ejector vs. time.

that the variation of expansion valve can cause obvious change of the pressure lift ratio, and the change trends of pressure lift ratio is reverse to that of the entrainment ratio. Thus, the expansion valve opening is an effective controlled objective for the constant pressure lift ratio of ejector.

The area ratio of ejector and expansion valve opening mainly influences the mass flow parameters and then spreads to the other system parameters. Comprehensive analysis on the simulation results above is conducted. With the increase of expansion valve opening, the mass flow rate through the expansion valve increases and the evaporator pressure increases. The gas cooler pressure decreases leading to the outlet pressure of primary nozzle decrease. Because the inlet pressure of suction chamber (i.e. evaporator pressure) is higher than the outlet pressure of primary nozzle, the differential pressure between them is enlarged and the mass flow rate of secondary flow is increased. Then, with the rise of evaporator pressure, the differential pressure between the separator and evaporator decreases, which begins to reduce the mass flow rate of expansion valve. The system gradually restores stability through its autoregulation, and the mass flow rate of expansion is equal to the secondary flow rate as well as the compressor flow rate is equal to the primary flow rate. When the area ratio of the ejector increases, the flow area of primary flow reduces which makes the primary flow rate decrease, leading to the increase of gas cooler pressure and the reduction of secondary flow rate. Due to the differential flow rate between the primary flow and the compressor flow, the gas cooler pressure appears the overshoot during the dynamic process. The decrease of mass flow rates into the separator results in the separator pressure decline. Due to the improvement of the differential pressure between gas cooler and separator, the compressor mass flow rate decreases. Then with the increase of gas cooler pressure, the primary flow rate begins to increase until it equals the compressor mass flow rate.

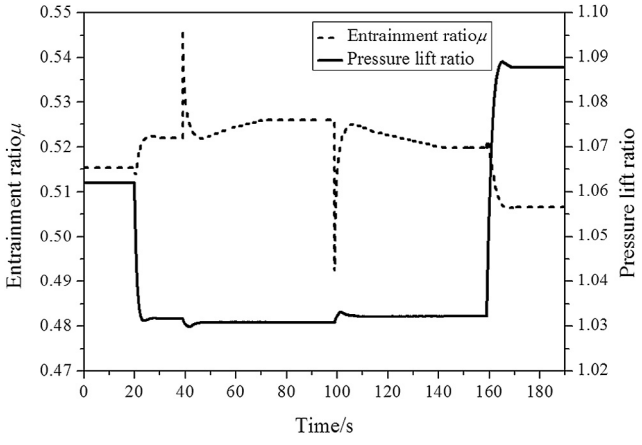

Fig. 14 – Entrainment ratio and pressure lift ratio of ejector vs. time.

5. Conclusions

This paper presents a numerical model to simulate the dynamic behavior of a transcritical CO_2 ejector expansion refrigeration cycle (EERC), which helps to understand the interactions among different components. The system models are developed based on the conservation of mass and energy. The numerical predictions are compared with the experimental data and the results show that the proposed model can accurately predict the system performances.

The dynamic responses on the pressures of gas cooler, evaporator and separator, mass flow rates, entrainment ratio and pressure lift ratio are simulated with different expansion valve opening and the ejector area ratios (the ratio of the area of mixing section to the area of primary nozzle throat). In general, the decrease of expansion valve opening or the increase of ejector area ratio causes the gas cooler pressure increase while evaporator pressure and separator pressure decrease. The area ratio of the ejector has greater effect on gas cooler pressure, while the valve opening influences the evaporator pressure more greatly. When the expansion valve opening increases, the mass flow rates of expansion valve, secondary flow, compressor and primary flow increase, while these mass flow rates decrease if the area ratio of ejector increases. The entrainment ratio has the same change direction with the expansion valve opening and the ejector area ratio, namely expansion valve opening or area ratio of ejector increases leading to the entrainment ratio rise, while the change of pressure lift ratio is inverse to that of entrainment ratio.

An improved understanding of the characteristics of the EERC is provided by the case of variation of expansion valve opening and the ejector area ratio. Other impacts of inner parameters and outer parameters can also be predicted based on the presented model. Although the dynamic model of EERC is developed and the dynamic analyses of the system are conducted, the system performance has not been discussed. We will design advantage control method based on the dynamic model to improve the system performance in the future work.

Acknowledgment

This work was supported by the National Natural Science Foundation of China (Grant No. 51076120).

REFERENCES

Bartosiewicz, Y., Aidoun, Z., Desevaux, P., Mercadier, Y., 2005. Numerical and experimental investigation on supersonic ejectors. Int. J. Heat Fluid Flow 26, 56–70.

Bendapudi, S., Braun, J.E., 2002. A review of literature on dynamic models of vapor compression equipment. ASHRAE Report, No. 4036–5.

Cardemil, J.M., Colle, S., 2012. A general model for evaluation of vapor ejectors performance for application in refrigeration. Energy Convers. Manage. 64, 79–86.

Cecchinato, L., Mancini, F., 2012. An intrinsically mass conservative switched evaporator model adopting the moving-boundary method. Int. J. Refrigeration 35, 349–364.

Cen, J.W., Liu, P., Jiang, F.M., 2012. A novel transcritical CO_2 refrigeration cycle with two ejectors. Int. J. Refrigeration 35, 2233–2239.

Chen, G.M., Xu, X.X., Li, S., Liang, L.X., Tang, L.M., 2010. An experimental and theoretical study of a CO_2 ejector. Int. J. Refrigeration 33, 915–921.

Chen, W., Chong, D., Yan, J., Liu, J., 2011. Numerical optimization on the geometrical factors of natural gas ejectors. Int. J. Therm. Sci. 50, 1554–1561.

Chen, W., Liu, M., Chong, D., Yan, J., Little, A.B., Bartosiewicz, Y., 2013. A 1D model to predict ejector performance at critical and sub-critical operational regimes. Int. J. Refrigeration 36, 1750–1761.

Dang, C.B., Hihara, E., 2004. In-tube cooling heat transfer supercritical carbon dioxide, Part1. Experimental measurement. Int. J. Refrigeration 27, 736–747.

Deng, J.Q., Jiang, P.X., Lu, T., Lu, W., 2007. Particular characteristics of transcritical CO_2 refrigeration cycle with an ejector. Appl. Therm. Eng. 27, 381–388.

Eames, I.W., Aphornratana, S., Haider, H., 1995. A theoretical and experimental study of a small-scale steam jet refrigerator. Int. J. Refrigeration 18, 378–386.

Eldredge, B.D., Rasmussen, B.P., Alleyne, A.G., 2008. Moving-boundary heat exchanger models with variable outlet phase. J. Dyn. Syst. Meas. Contr. 130, 061003.

Gnielinski, V., 1976. New equations for heat and mass transfer in turbulent pipe and channel flow. Int. Chem. Eng. 16, 359–368.

He, Y., Deng, J.Q., Zhang, Z.X., 2014. Thermodynamic study on a new transcritical CO_2 ejector expansion refrigeration system with two-stage evaporation and vapor feedback. HVAC&R Res. 20, 655–664.

Huang, B.J., Chang, J.M., Wang, C.P., Petrenko, V.A., 1999. A 1-D analysis of ejector performance. Int. J. Refrigeration 22, 354–364.

Hwang, Y., 1997. Comprehensive Investigation of Carbon Dioxide Refrigeration Cycle (Ph.D. dissertation). University of Maryland, College Park.

Jesen, J.M., Tummescheit, H.M., 2002. Moving boundary models for dynamic simulations of two-phase flows. In: Proceedings of Second International Modelica Conference, Oberpfaffenhofen, Germany, pp: 235–244.

Koury, R.N.N., Faria, R.N., Nunes, R.O., Ismail, K.A.R., Machado, L., 2013. Dynamic model and experimental study of an air–water heat pump for residential use. Int. J. Refrigeration 36, 674–688.

Li, D.G., Groll, E.A., 2005. Transcritical CO_2 refrigeration cycle with ejector-expansion device. Int. J. Refrigeration 28, 766–773.

Little, A.B., Bartosiewicz, Y., Garimella, S., 2012. Optical validation of ejector flow characteristics predicted by computational analysis. In: Proceedings of the IMECE 2012: ASME International Mechanical Engineering Congress & Exposition, Houston, Texas, USA.

Liu, F., Groll, E.A., 2013. Study of ejector efficiencies in refrigeration cycles. Appl. Therm. Eng. 52, 360–370.

Liu, F., Groll, E.A., Li, D.Q., 2012. Modeling study of an ejector expansion residential CO_2 air conditioning system. Energ. Buildings 53, 127–136.

McLinden, M.O., Klein, S.A., Lemmon, E.W., Peskin, A.P., 2002. NIST Reference Fluid Thermodynamics and Transport Properties "REFPROP", National Institute of Standards and Technology. U.S. Department of Commerce, Gaithersburg.

Pettit, N.B.O.L., Willatzen, M., Plong-Sørensen, L., 1998. A general dynamic simulation model for evaporators and condensers in refrigeration part I: moving boundary formulation of two-phase flows with heat exchange. Int. J. Refrigeration 21, 398–404.

Pfafferott, T., Schmitz, G., 2004. Modelling and transient simulation of CO_2-refrigeration systems with Modelica. Int. J. Refrigeration 27, 42–52.

Rasmussen, B.P., 2002. Control-Oriented Modeling of Transcritical Vapor Compression Systems (Master thesis). University of Illinois, Urbana-Champaign.

Rasmussen, B.P., Alleyne, A.G., Musser, A.B., 2005. Model-driven system identification of transcritical vapor compression system. IEEE Trans. Control Syst. Technol. 13, 444–451.

Rice, C.K., 1987. The effect of void fraction correlation and heat flux assumption on refrigerant charge inventory predictions. ASHRAE Trans. 93, 341–367.

Sarkar, J., 2008. Optimization of ejector-expansion transcritical CO_2 heat pump cycle. Energy 33, 1399–1406.

Sarkar, J., Bhattacharyya, S., Gopal, M.R., 2006. Simulation of a transcritical CO_2 heat pump cycle for simultaneous cooling and heating applications. Int. J. Refrigeration 29, 735–743.

Schurt, L.C., Hermes, C.J.L., Neto, A.T., 2009. A model-driven multivariable controller for vapor compression refrigeration systems. Int. J. Refrigeration 32, 1672–1682.

Shi, R.F., Fu, D.G., Feng, Y.S., Fan, J.Q., Mijanovic, S., Radcliff, T., 2010. Dynamic Modeling of CO_2 Supermarket Refrigeration System. International Refrigeration and Air Conditioning Conference. Paper 1127.

White, F.M., 2009. Fluid Mechanics, sixth ed. McGraw-Hill, New York.

Xu, X.X., Chen, G.M., Tang, L.M., Zhu, Z.J., 2012. Experimental investigation on performance of transcritical CO_2 heat pump system with ejector under optimum high-side pressure. Energy 44, 870–877.

Yari, M., 2009. Performance analysis and optimization of a new two-stage ejector-expansion transcritical CO_2 refrigeration cycle. Int. J. Therm. Sci. 48, 1997–2005.

Zhang, W.J., Zhang, C.L., 2006. A generalized moving-boundary model for transient simulation of dry-expansion evaporators under larger disturbances. Int. J. Refrigeration 29, 1119–1127.